AIP | Journal of Applied Physics

Effects of the surface charge screening and temperature on the vortex domain patterns of ferroelectric nanodots

C. M. Wu, W. J. Chen, D. C. Ma, C. H. Woo, and Yue Zheng

Citation: J. Appl. Phys. **112**, 104108 (2012); doi: 10.1063/1.4766382
View online: http://dx.doi.org/10.1063/1.4766382
View Table of Contents: http://jap.aip.org/resource/1/JAPIAU/v112/i10
Published by the AIP Publishing LLC.

Effects of the surface charge screening and temperature on the vortex domain patterns of ferroelectric nanodots

C. M. Wu,[1] W. J. Chen,[1] D. C. Ma,[1] C. H. Woo,[2] and Yue Zheng[1,a)]
[1]*State Key Laboratory of Optoelectronic Materials and Technologies, Micro & Nano Physics and Mechanics Research Laboratory, School of Physics and Engineering, Sun Yat-sen University, 510275 Guangzhou, China*
[2]*Department of Electronic and Information Engineering, The Hong Kong Polytechnic University, Hong Kong*

(Received 16 August 2012; accepted 20 October 2012; published online 21 November 2012)

Based on the phase field simulations, effects of the surface charge screening and temperature on the vortex domain structure of the ferroelectric nanodot have been investigated. Our calculations show that the ferroelectric nanodot adopts a rhombohedral vortex domain pattern under an ideal open-circuit boundary condition. With the increase of the surface charge screening, the dipole vortex gradually rotates and appears rhombohedral-orthorhombic-tetragonal transformation. By adjusting the surface charge screening, the polar single domain and multi-vortices domain patterns with zero toroidal moment have been obtained near the phase transition temperature. More importantly, temperature and charge screening "T-C" phase diagram has been summarized, which indicates an effective method to control the vortex domain structure in the low-dimensional ferroelectric nanostructures. © *2012 American Institute of Physics*. [http://dx.doi.org/10.1063/1.4766382]

I. INTRODUCTION

Ferroelectric materials have attracted considerable attentions due to their functional properties, e.g., ferroelectricity, piezoelectricity, and photoelectricity, etc., which present attractive prospects of applications in memories, actuators, sensors, and photonic devices.[1–7] Particularly, due to effects of size, surface, and interface, ferroelectric nanostructures may be quite different in property from their bulk counterparts.[8–13] The small size, high surface-volume ratio, and inherent functional properties of ferroelectric nanostructures are important in developing functional nanodevices and device miniaturization. Currently, ferroelectric nanostructures can be experimentally prepared by various synthesis methods, and have been reported in a large amount of papers in order to utilize them in nanodevices.[14,15] Large quantities of theoretical approaches, i.e., thermodynamic modeling, atomistic level simulations, and first-principle calculations, etc., are focused on studying properties of ferroelectric nanostructures, and want to reveal the finite size effect on ferroelectricity, domain structure and related properties.[16–22]

Recent theoretical simulations and experimental results have shown that ferroelectric nanostructures can exhibit toroidal order of ferroelectric domains.[23–28] This so-called vortex domain structure (VDS) is likely to be induced by strong geometric confinements or coupling between order parameters. The distinct characteristics of VDS and the novel ways to control it should provide exciting opportunities in designing novel functional devices. For example, with controlling the vortex pattern such as its chirality, it is promising to use the nanostructures as basic memory cells and increase ferroelectric nonvolatile-memory density. In literature, mechanisms of forming VDS and effects of many factors on VDS in ferroelectric nanostructures have been theoretically studied.[18,29–31] Using electron microscopy or high resolution piezoresponse force microscopy (PFM), experiments were also close to definitely characterize nanoscale ferroelectric vortices.[25,28,32–34] Nevertheless, in contrast to the intensive study on magnetic VDS, research on VDS in ferroelectric nanostructures is still in its infancy. Many problems of ferroelectric VDS require further investigation. Discovering regular controllability on the VDS in ferroelectric nanostructures is important for future applications.

It is well known that the electric boundary condition plays an important role in the formation and stability of domain structures in ferroelectrics. Uncompensated bound charges at surface and interface of ferroelectrics can induce remarkable depolarization field. To minimize total energy induced by such a large depolarization field, domain patterns such as 180° domains and toroidal polarization domains are likely to form. The strong effects of the electric boundary condition on the domain structures in ferroelectric nanostructures have been investigated extensively.[23,35] As one of the remarkable findings, recent investigations showed that large amount of low-dimensional ferroelectric nanostructures could appear vortex domain patterns when they are subjected to ideal or near open-circuit boundary condition.[22,23,30] Strong dependences of this phenomenon on the dimensionality, geometry, and size of the ferroelectric nanostructures were further reported.[22,27,30,36] More recently, using the first-principle-based effective Hamiltonian method, Prosandeev *et al.*[37] proposed an efficient control of the vortex orientation by placing charged tips near the ferroelectric nanodots. It should be noted that previous investigations mainly concentrated on the effect of various electric boundary conditions on the formation of VDS in ferroelectric nanostructures. Nevertheless, how the formed VDS evolves when the boundary condition changes has not been investigated. This issue is also fundamental and important for applications of ferroelectric nanostructures with VDS.

In this work, we report that the VDS of ferroelectric nanodot indeed can exhibit regular response to controllable

a)Author to whom correspondence should be addressed. Electronic mail: zhengy35@mail.sysu.edu.cn.

charge screening by phase field simulations. The phase field model is based on a Landau-Devonshire-Ginzburg (LDG) free-energy, which takes into account the effects of inhomogeneous electromechanical fields. The VDS of a ferroelectric nanodot under ideal open-circuit boundary condition and the effects of charge screening and temperature on the formed VDS are systematically investigated. The temperature and charge screening "T-C" phase diagram for ferroelectric nanodot will be summarized and discussed.

II. THE PHYSICAL MODEL

The advantage of phase field model over conventional thermodynamic approaches is that it does not need to make any a prior assumption with regard to the possible domain wall orientations for predicting the domain structures.[8] In our phase field model, the spontaneous polarization $\mathbf{P} = (P_1, P_2, P_3)$ is considered as the order parameter, which is generated by the spontaneous atomic displacements in a dielectric when a ferroelectric phase transition occurs. The electric displacement field $\mathbf{D}$ is expressed as a function of the electric field and spontaneous polarization, i.e., $\mathbf{D} = \boldsymbol{\varepsilon}_\mathbf{b}\mathbf{E} + \mathbf{P}$, where $\mathbf{E}$ is the electric field and $\boldsymbol{\varepsilon}_\mathbf{b}$ is the background dielectric constant tensor.[38–40] From this construction, the displacement field has been decomposed into linear and nonlinear parts, which is important for appropriate construction of the thermodynamic free energy of ferroelectric nanostructures. Since the background material is the paraelectric phase of a cubic crystal structure, the background dielectric constants along the axial directions are same, i.e., $\varepsilon_b = \varepsilon_{11b} = \varepsilon_{22b} = \varepsilon_{33b}$.

The temporal evolution of the domain structures is characterized by evolution of the polarization field. It can be phenomenologically described by well known time-dependent Ginzburg-Landau (TDGL) equation, i.e.,

$$\frac{\partial P_i}{\partial t} = -M\frac{\delta F}{\delta P_i} \quad (i = 1, 2, 3), \tag{1}$$

which assumes that the change of order parameter field is proportional to the variation of the system's free energy with respect to the order parameter. In the above expression, F is the total free energy of the ferroelectric nanodot, t is the time, and M is the kinetic coefficient related to the domain wall mobility.

In order to investigate the domain structures of a ferroelectric system in nanoscale, it is important to take into account the inhomogeneous electromechanical fields and the effects of surface and interface. Following the previous works,[18,46] the total free energy of the ferroelectric system can be generally expressed as functions of polarization, polarization gradient, electric field, and mechanical field. We express the free energy of the ferroelectric nanodot as a sum of the Landau-Devonshire energy, gradient energy, electrostatic energy, and surface energy, i.e.,

$$F = \int_V (f_{\mathrm{LD}} + f_{\mathrm{grad}} + f_{\mathrm{elec}})dV + \int_S f_{\mathrm{surf}}dS, \tag{2}$$

where V and S are the volume and surface of nanodot, f_{LD}, f_{grad}, f_{elec}, and f_{surf} are densities of the Landau-Devonshire energy, gradient energy, electric energy, and the surface energy, respectively.

Under the condition of applied stress, the Landau-Devonshire energy density f_{LD} should be a function of the spontaneous polarization and stress. In this work, an eighth-order polynomial of the modified Landau-Devonshire energy density is adopted as[41–43]

$$\begin{aligned} f_{\mathrm{LD}} = {} & \alpha_1(P_1^2 + P_2^2 + P_3^2) + \alpha_{11}(P_1^4 + P_2^4 + P_3^4) + \alpha_{12}(P_1^2P_2^2 + P_2^2P_3^2 + P_1^2P_3^2) \\ & + \alpha_{111}(P_1^6 + P_2^6 + P_3^6) + \alpha_{112}[P_1^2(P_2^4 + P_3^4) + P_2^2(P_1^4 + P_3^4) + P_3^2(P_1^4 + P_2^4)] \\ & + \alpha_{123}P_1^2P_2^2P_3^2 + \alpha_{1111}(P_1^8 + P_2^8 + P_3^8) + \alpha_{1112}[P_1^6(P_2^2 + P_3^2) + P_2^6(P_1^2 + P_3^2) \\ & + P_3^6(P_1^2 + P_2^2)] + \alpha_{1122}(P_1^4P_2^4 + P_2^4P_3^4 + P_1^4P_3^4) + \alpha_{1123}(P_1^4P_2^2P_3^2 + P_2^4P_1^2P_3^2 \\ & + P_3^4P_1^2P_2^2) - Q_{11}(\sigma_{11}P_1^2 + \sigma_{22}P_2^2 + \sigma_{33}P_3^2) - Q_{12}[(\sigma_{11}(P_2^2 + P_3^2) + \sigma_{22}(P_1^2 + P_3^2) \\ & + \sigma_{33}(P_1^2 + P_2^2)] - Q_{44}(\sigma_{12}P_1P_2 + \sigma_{13}P_1P_3 + \sigma_{23}P_2P_3) - \frac{1}{2}s_{11}(\sigma_{11}^2 + \sigma_{22}^2 + \sigma_{33}^2) \\ & - s_{12}(\sigma_{11}\sigma_{22} + \sigma_{22}\sigma_{33} + \sigma_{11}\sigma_{33}) - \frac{1}{2}s_{44}(\sigma_{12}^2 + \sigma_{23}^2 + \sigma_{13}^2), \end{aligned} \tag{3}$$

where $\alpha_1 = (T - T_0)/(2\varepsilon_0 C_0)$ is the dielectric stiffness, T_0 and C_0 are the Curie-Weiss temperature and Curie-Weiss constant, respectively, ε_0 is the vacuum permittivity, and T is the temperature. α_{ij}, α_{ijk} and α_{ijkl} are the higher-order dielectric stiffness coefficients. Q_{ij} and s_{ij} are the electrostrictive and elastic compliance coefficients, respectively. σ_{ij} are the stress components and should be determined by the mechanical equilibrium equation, i.e., $\sigma_{ij,j} = 0$, with the comma in the subscript denoting the spatial differentiation. When the nanodot is free-standing, the mechanical boundary condition at the surface is given by $\sigma_{ij}n_j = 0$, with n_j being the j-component of the unit vector normal to the surface.

The gradient energy is determined by the spatial variation of the polarization in ferroelectric nanodot. To the lowest order Taylor expansion, the gradient energy density f_{grad} can be written as

$$f_{\text{grad}}(P_{i,j}) = \frac{1}{2}G_{11}(P_{1,1}^2 + P_{2,2}^2 + P_{3,3}^2) + G_{12}(P_{1,1}P_{2,2} + P_{2,2}P_{3,3} + P_{1,1}P_{3,3}) + \frac{1}{2}G_{44}[(P_{1,2} + P_{2,1})^2 + (P_{2,3} + P_{3,2})^2 + (P_{1,3} + P_{3,1})^2] + \frac{1}{2}G'_{44}[(P_{1,2} - P_{2,1})^2 + (P_{2,3} - P_{3,2})^2 + (P_{1,3} - P_{3,1})^2], \quad (4)$$

where G_{11},G_{12},G_{44}, and G'_{44} are gradient energy coefficients.

When there is absent of external electric field, the total electric field of a nanodot is the depolarization field. Such a depolarization field is induced by the spatial variation of polarization and incomplete screening of the polarization charges at the surface and interface of the nanodot. According to the previous works,[38,39,44] the electric energy density of a given polarization distribution is given by $f_{elec} = -P_1E_1 - P_2E_2 - P_3E_3 - \frac{1}{2}\varepsilon_b(E_1^2+E_2^2+E_3^2)$. For simplicity, in this work, we consider that the ferroelectric nanodot is a body-charge-free system. It is expected that the nanodot would undergo a maximum depolarization field $\mathbf{E}^{\text{op}} = (E_1^{\text{op}}, E_2^{\text{op}}, E_3^{\text{op}})$ when it is under an ideal open-circuit boundary condition since no polarization charge is compensated by the external free charges. $\mathbf{E}^{\text{op}}$ can be obtained from the electrostatic equilibrium equation, i.e., $\mathbf{D}_{i,i} = (\varepsilon_b\mathbf{E} + \mathbf{P})_{i,i} = 0$, together with the boundary condition $D_i n_i = 0$. As charge screening tends to decrease the depolarization field inside the nanodot, the electric field of a nanodot with charge screening can be approximately calculated by $\mathbf{E} = (\beta_1 E_1^{\text{op}}, \beta_2 E_2^{\text{op}}, \beta_3 E_3^{\text{op}})$, where β_i are screening factors along different directions. With β_i varying from zero to one, we can mimic the different charge screening conditions from the complete screening boundary condition ($\beta_i = 0$) to the ideal open-circuit boundary condition ($\beta_i = 1$). Note that the charge screening of a real ferroelectric nanodot can be controlled either by the charges in the electrodes or by ionic surface compensation through chemical equilibrium with an environment.[45–47] In both cases, the screening factor β_i should be strong functions of experimental variables controlling the amount and distribution of the screening charges. Nevertheless, it is not our purpose to model the dependences of β_i on the experimental variables but to give a qualitative prediction of the charge screening effect on the VDS of ferroelectric nanodot.

The polarization is inhomogeneous owing to the truncation near surfaces. Thus, an additional surface energy is necessary to describe this intrinsic effect. Using the extrapolation length δ_i,[48] the surface energy density is given by $f_{\text{surf}} = \frac{D_{11}P_1^2}{2\delta_1} + \frac{D_{22}P_2^2}{2\delta_2} + \frac{D_{44}P_3^2}{2\delta_3}$, where D_{ij} are the material coefficients related to the gradient energy coefficients and surface orientation.

III. RESULTS AND DISCUSSIONS

In the following calculations, we take the free-standing $BaTiO_3$ nanodot with charge screening at the top and bottom surfaces (i.e., $\beta_1 = \beta_2 = 1, 0 \le \beta_3 \le 1$) as example to demonstrate the charge screening effect on the VDS of the ferroelectric nanostructures. A meshing of $10 \times 10 \times 10$ elements at a scale of $\Delta x = \Delta y = \Delta z = 0.4$ nm is used to simulate a cubic nanodot.

The evolution of polarization is solved by discretizing the TDGL equation in time. Assume that the system reaches mechanical and electric equilibrium instantaneously once the spontaneous polarization distribution is set down. Therefore, at each time step, the stress field and electrostatic field can be obtained by solving the mechanical equilibrium equation and electrostatic equilibrium equation with the polarization obtained at the last time step. Finite element methods are used to solve the mechanical and electrostatic equilibrium equations. Values of the expansion coefficients of the eighth-order Landau-Devonshire potential, electrostrictive coefficients, elastic properties,[42,49,50] and extrapolation length[51] in the simulations are listed in Ref. 52.

A. Vortex domain structures under the ideal open-circuit boundary condition

We would like to start simulations on VDS of a nanodot under the ideal open-circuit boundary condition, the results of which can be compared with the posterior ones of charge screening. A random perturbation of polarization field is introduced to initiate the polarization evolution, and the polarization field can evolve to the stable state after iterative calculation according to the TDGL equation. To fully characterize various domain patterns that might be toroidal or polar, we would give plots of the domain patterns and calculate their average polarization vector $\bar{\mathbf{P}}$ and the toroidal moment, i.e., $\mathbf{g} = \frac{1}{V}\int_V \mathbf{r} \times (\mathbf{P} - \bar{\mathbf{P}})dV$,[53] with $\mathbf{r}$ being the position vector. The average magnitude of the polarization at all the sites,

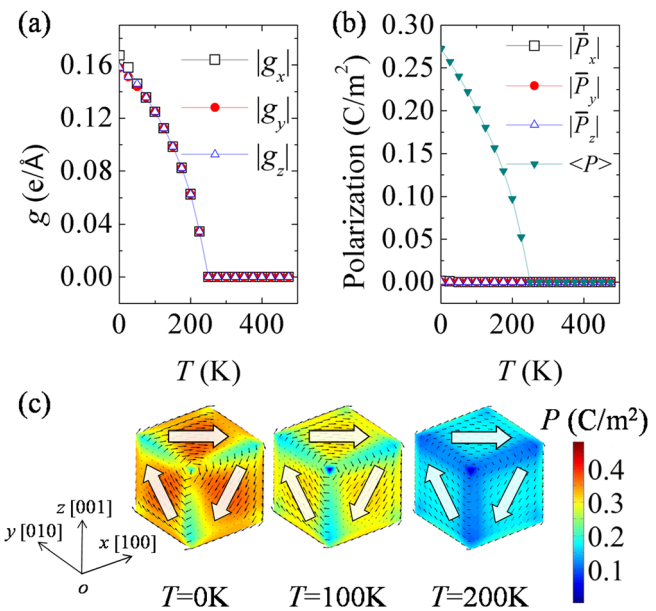

FIG. 1. Simulated results of a ferroelectric nanodot under ideal open-circuit boundary condition. (a) $|g_x|$, $|g_y|$, $|g_z|$, (b) $|\bar{P}_x|$, $|\bar{P}_y|$, $|\bar{P}_z|$ and $\langle P \rangle$, and (c) the equilibrium domain structures.

i.e., $\langle P\rangle$=mean($\sqrt{P_1^2+P_2^2+P_3^2}$), is calculated to denote the paraelectric-ferroelectric transition.

The simulated result of the domain structure of a nanodot at different temperatures is shown in Fig. 1. When temperature is lower than ~240 K, the toroidal moment components of the stable domain structure are found nonzero and keep almost equal with each other (see Fig. 1(a)). Actually, minor differences between the toroidal moment components could be identified near 0 K. It can be also seen that the toroidal moment components decrease as the temperature increases, which is in accordance with the average magnitude of the polarization changing shown in Fig. 1(b). Note that the average magnitude of the polarization is nonzero when the temperature is lower than ~240 K. However, the polarization of the system, $\bar{\mathbf{P}}$, keeps near-null at all temperatures. By plotting the morphologies of equilibrium domain structures at different temperatures as shown in Fig. 1(c), we found that the nanodot actually adopts a rhombohedral vortex domain pattern ($|g_x| \approx |g_y| \approx |g_z|$) with its vortex axis along the $\langle 111\rangle$ directions when the temperature is lower. As mentioned above, the vortex domains are formed to decrease the large depolarization field caused by open-circuit boundary condition. This result is similar to that obtained by using an effective Hamiltonian simulation.[53]

B. Effects of charge screening and temperature on vortex domain structures

The above result shows that adjusting the ambient temperature significantly affects the magnitude of the toroidal moment of the nanodot under the ideal open-circuit condition, wherein the domain structure still keeps a rhombohedral-type vortex domain pattern. It is interesting to see how the rhombohedral vortex domain pattern evolves if the charge screening condition departs from the ideal open-circuit condition. Furthermore, the ambient temperature should also play an important role in the evolution. To demonstrate this, we further simulate the nanodot under various charge screening conditions and temperatures. The initial domain patterns of the nanodot are those obtained from random perturbation under the ideal open-circuit condition (see Fig. 1).

As shown in Fig. 2, a significant charge screening effect on VDS can be found at $T = 50$ K. With the screening factor β_3 decreasing from 1 to 0, the vortex axis of the initial rhombohedral vortex domain pattern tends to rotate to the x-y plane, and continuous transformations into orthorhombic-like (i.e., $|g_x| \simeq |g_y| \gg |g_z|$) and tetragonal-like (i.e., $|g_x| \gg |g_{y,z}|$) vortex domain patterns are observed. Particularly, transformation into orthorhombic-like vortex domain pattern takes place as β_3 decreases to a critical value, i.e., ~0.16. During the transformation, the z-component of the toroidal moment of the domain pattern $|g_z|$ keeps decreasing, meanwhile the other two components keep equal and increasing (Fig. 2(a)). As β_3 further decreases, $|g_y|$ also becomes to decrease and $|g_x|$ keeps increasing, indicating that transformation into tetragonal-like vortex domain pattern happens. From Fig. 2(b), we can note that the average polarization magnitude $\langle P\rangle$ increases as β_3 decreases and the net polarization vector of the system keeps null, indicating that no polar domain pattern appears. It can be also seen that as β_3 changes from 1 to 0, the toroidal moment components remain nonzero, due to the fact that rhombohedral phase tends to form at the low temperature. This can be further verified from the domain morphologies at different screening conditions as shown in Fig. 2(c). We can see from these results that, as the charge screening along z-direction increasing, the toroidal axis of the dipole vortex tends to rotate to x or y-direction. The reason is that the decrease of depolarization field along z-direction makes the polarization dipoles favor them along this direction.

To see the combining effect of temperature and charge screening, simulations of a nanodot under variable charge screening at other temperatures are constructed. Figs. 3 and

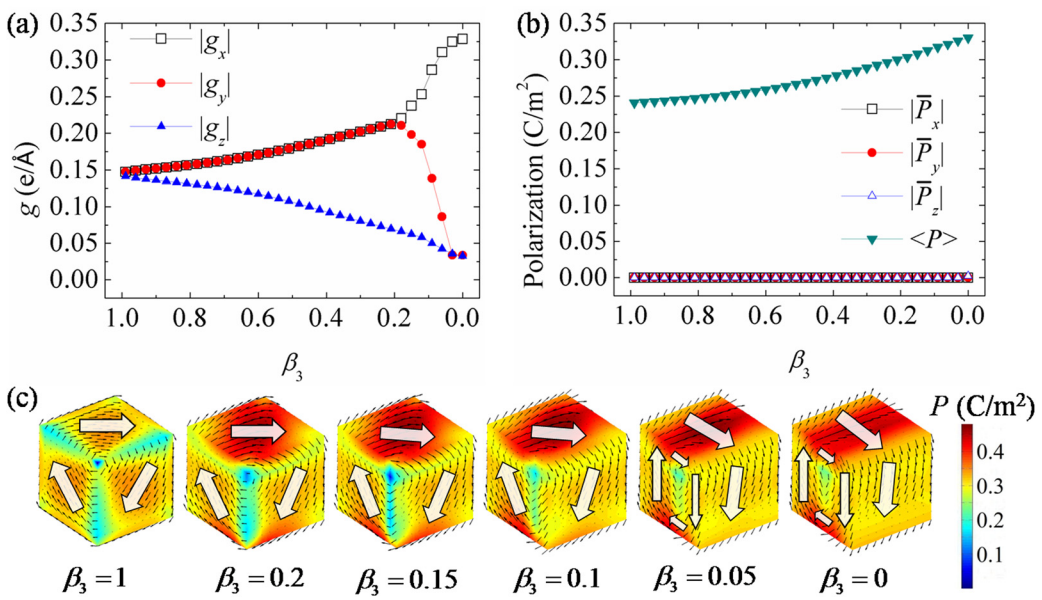

FIG. 2. Simulated results of a ferroelectric nanodot at the temperature of 50 K as functions of charge screening factor β_3. (a) $|g_x|$, $|g_y|$, $|g_z|$, (b) $|\bar{P}_x|$, $|\bar{P}_y|$, $|\bar{P}_z|$ and $\langle P\rangle$, and (c) the equilibrium domain structures.

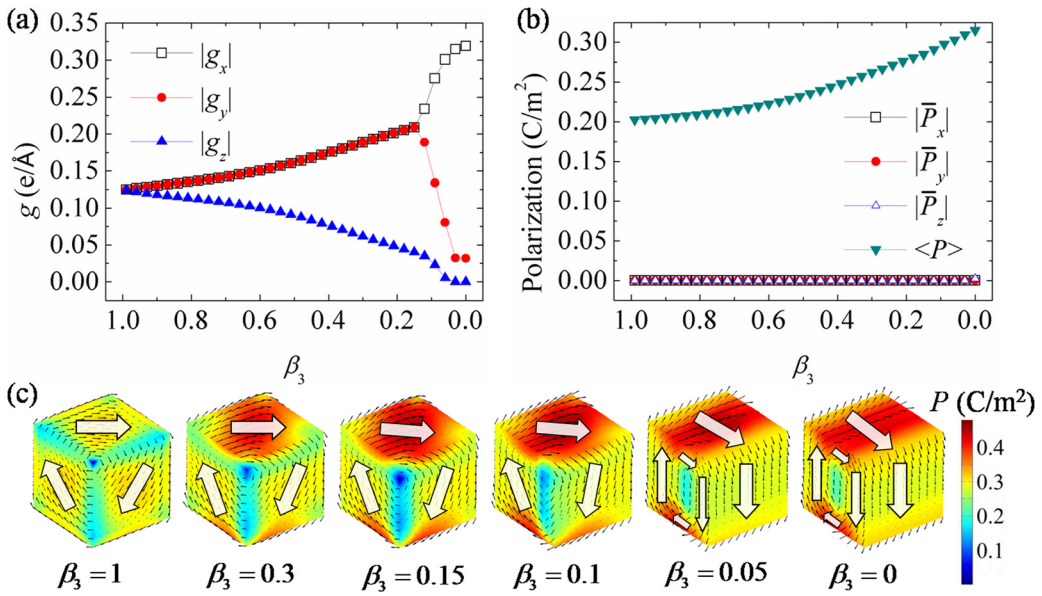

FIG. 3. Simulated results of a ferroelectric nanodot at the temperature of 100 K as functions of charge screening factor β_3. (a) $|g_x|$, $|g_y|$, $|g_z|$, (b) $|\bar{P}_x|$, $|\bar{P}_y|$, $|\bar{P}_z|$ and $\langle P \rangle$, and (c) the equilibrium domain structures.

4 depict the results of $T = 100$ K and 200 K, respectively. For nanodot at $T = 100$ K, the evolution of the domain pattern is quite similar to that of $T = 50$ K. However, the critical screening factors of the transformations have changed a little bit. For example, the critical screening factor of transformation from the initial rhombohedral vortex domain pattern into tetragonal-like vortex domain pattern decreases to be 0.13. Moreover, we find $|g_z|$ can reach zero as β_3 is sufficient small, which indicates that the vortex axis of the evolved domain pattern is on the *x*-*y* plane. When temperature rises to 200 K, the evolution of the domain pattern becomes even more fruitful as shown in Fig. 4. In this case, the initial rhombohedral vortex domain pattern gradually transforms into a perfect orthorhombic vortex domain pattern (i.e., $|g_x| = |g_y|, |g_z| = 0$) as the screening factor β_3 decreases to 0.34, and it becomes tetragonal-like for $\beta_3 \approx 0.06$ (Fig. 4(a)). Moreover, due to the relatively small polarization at 200 K and the strongest charge screening, a polar single-domain structure appears under the complete screening boundary condition, with $|g_x| = |g_y| = |g_z| = 0$ and a net polarization equal to 0.28 C/m^2 along the *z*-direction (Fig. 4(b)).

When temperature reaches 250 K, which is near the ferroelectric-paraelectric transition temperature of the nanodot, the polarization magnitude of each site is quite small under the open-circuit boundary condition (see Fig. 1). Using this polarization distribution as initial value, we further simulate the domain pattern with variable charge screening condition, and give result in Fig. 5. It can

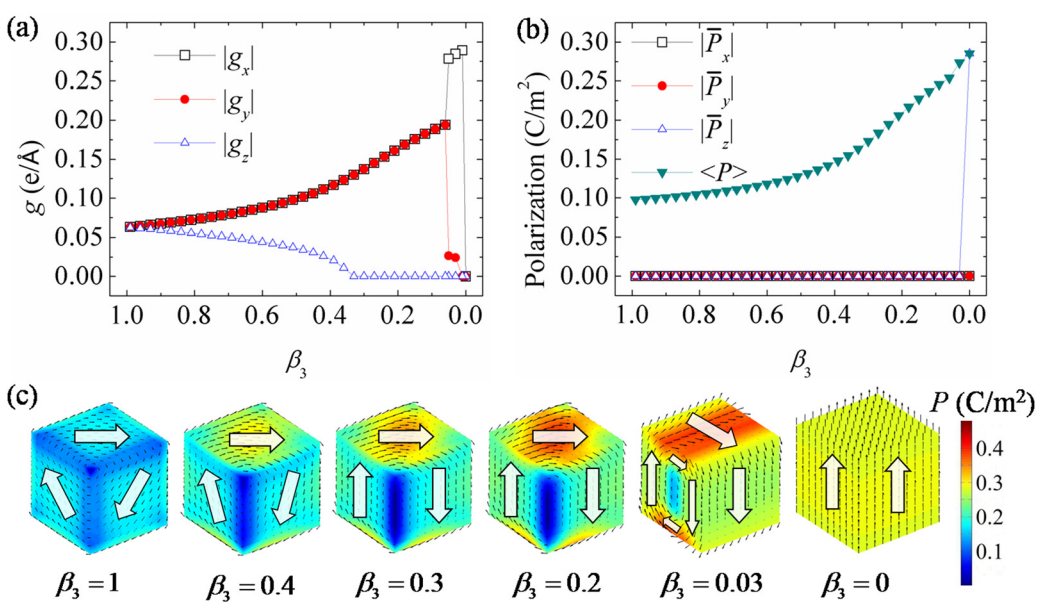

FIG. 4. Simulated results of a ferroelectric nanodot at the temperature of 200 K as functions of charge screening factor β_3. (a) $|g_x|$, $|g_y|$, $|g_z|$, (b) $|\bar{P}_x|$, $|\bar{P}_y|$, $|\bar{P}_z|$ and $\langle P \rangle$, and (c) the equilibrium domain structures.

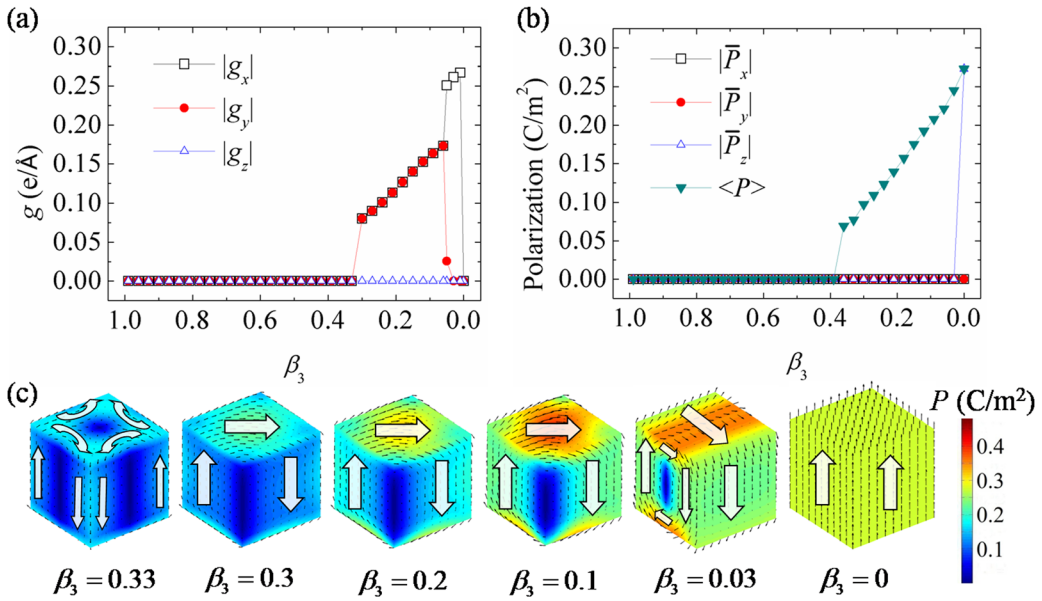

FIG. 5. Simulated results of a ferroelectric nanodot at the temperature of 250 K as functions of charge screening factor β_3. (a) $|g_x|$, $|g_y|$, $|g_z|$, (b) $|\bar{P}_x|$, $|\bar{P}_y|$, $|\bar{P}_z|$ and $\langle P \rangle$, and (c) the equilibrium domain structures.

be seen from Figs. 5(a) and 5(b) that both the toroidal moment and the polarization of the nanodot are near-null for the screening factor β_3 in-between 1 and 0.38. However, when β_3 falls into a region between 0.38 and 0.31, the average polarization magnitude $\langle P \rangle$ becomes nonzero whereas the toroidal moment remains near-null. This indicates that a new phase transition happens. From Fig. 5(c), we indeed find that the nanodot adopts a domain pattern with 4-vortices. The four vortices have their toroidal axes, respectively, along $[\bar{1}00]$, [100], $[0\bar{1}0]$, and [010] directions, and the polarization dipoles are mainly along the z-axis. The toroidal moments of four vortices are equal in magnitude so that no net toroidal moment is exhibited. As β_3 further decreases, the nanodot subsequently adopts orthorhombic-like and tetragonal-like vortex domain patterns similar to the results at previous investigated temperatures. A polar single-domain structure is also found at complete screening boundary condition.

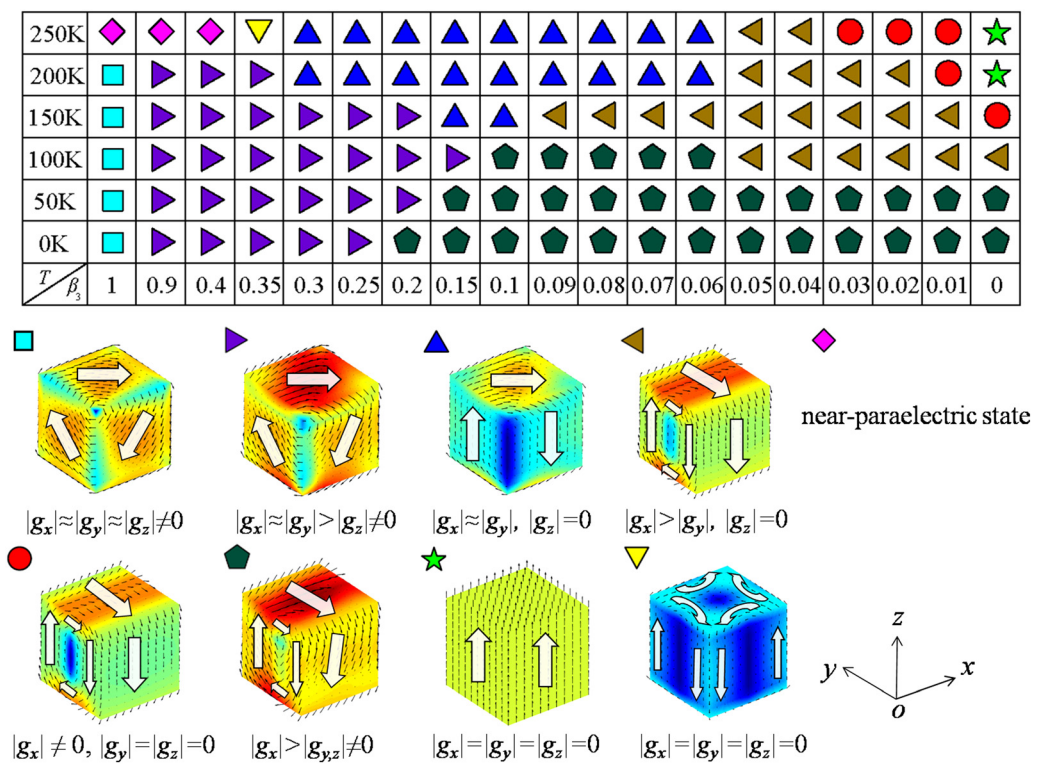

FIG. 6. Phase diagram depicting the domain pattern of the nanodot as a function of temperature and charge screening factor β_3.

C. Temperature and charge screening "T-C" phase diagram

To understand the charge screening and temperature effects more clearly, we plot the "T-C" phase diagram as shown in Fig. 6, which depicts the domain pattern of the nanodot as functions of temperature and charge screening factor β_3. The initial domain patterns are those obtained under the ideal open-circuit condition, i.e., $\beta_3 = 1$. The domain structures represented by the symbols are schematically depicted. Note that we have generally classified up to seven vortex domain patterns according to the relative magnitudes of the toroidal moment components.

Fruitful control on the domain pattern of ferroelectric nanodot by the charge screening is clearly demonstrated in Fig. 6. At low temperatures, the evolved domain structures remain single vortex and the vortex axis tends to rotate to the *x-y* plane as the charge screening gradually increases. As a consequence, orthorhombic-like and tetragonal-like vortex domain patterns are obtained. Particularly, perfect orthorhombic and tetragonal domain patterns can be obtained at higher temperatures. At high temperature near-paraelectric region, domain structure with 4-vortices is found at moderate charge screening (e.g., $\beta_3 = 0.35$ at $T = 250$ K). Polar single-domain pattern is found to appear at higher temperature under complete charge screening boundary condition. These results clearly show that fruitful vortex domain patterns can be obtained from the formed vortex domain pattern by the combining control of charge screening and temperature. This regular response of ferroelectric VDS to the charge screening condition and the ambient temperature should have important indications in applying ferroelectric nanostructures to novel functional devices.

IV. CONCLUSIONS

In summary, we have investigated on the effects of surface charge screening and temperature on the VDS in free-standing ferroelectric nanodot based on the phase field simulations. Results show that the nanodot adopts rhombohedral vortex domain pattern under the ideal open-circuit boundary condition. Meanwhile, the formed rhombohedral vortex domain pattern can evolve into orthorhombic and tetragonal vortex domain patterns with increasing the charge screening at the bottom and top surfaces. Moreover, polar single domain and multi-vortices domain with zero toroidal moment can be obtained by adjusting charge screening at near phase transition temperature. The fruitful temperature and charge screening "T-C" phase diagram is summarized. The predicted transformations between vortex domain patterns indicate potential applications in nanoscale memories, sensors, or other functional nanodevices.

ACKNOWLEDGMENTS

The authors acknowledge the financial support of the National Natural Science Foundation of China (NSFC) (Nos. 10902128, 11072271, 50802026, 10972239, and 11232015). Yue Zheng also thanks support by the Fundamental Research Funds for the Central Universities, New Century Excellent Talents in University, Fundamental Research Funds for the Central Universities, Research Fund for the Doctoral Program of Higher Education, and Fok Ying Tung Foundation.

[1]O. Auciello, J. F. Scott, and R. Ramesh, Phys. Today **51**(7), 22 (1998).
[2]I. I. Naumov, L. Bellaiche, and H. Fu, Nature **432**, 737 (2004).
[3]A. N. Morozovska, E. A. Eliseev, M. D. Glinchuk, and R. Blinc, Phys. Rev. B **81**, 092101 (2010).
[4]T. N. Ng, D. E. Schwartz, L. L. Lavery, G. L. Whiting, B. Russo, B. Krusor, J. Veres, P. Bröms, L. Herlogsson, N. Alam, O. Hagel, J. Nilsson, and C. Karlsson, Sci. Rep. **2**, 585 (2012).
[5]T. H. E. Lahtinen, K. J. A. Franke, and S. van Dijken, Sci. Rep. **2**, 258 (2012).
[6]Y. Zheng and C. H. Woo, Nanotechnology **20**, 075401 (2009); X. Luo, B. Wang, and Y. Zheng, ACS Nano **5**, 1649 (2011).
[7]T. Chen and J. F. Scott, Integr. Ferroelectr. **3**, 69 (1993).
[8]Y. L. Li, S. Y. Hu, Z. K. Liu, and L. Q. Chen, Acta Mater. **50**, 395 (2002).
[9]Y. Zheng, C. H. Woo, and B. Wang, Nano Lett. **8**, 3131 (2008)
[10]N. A. Pertsev, A. G. Zembilgotov, and A. K. Tagantsev, Phys. Rev. Lett. **80**, 1988 (1998).
[11]Y. Zheng, S. P. Lin, and B. Wang, Appl. Phys. Lett. **99**, 062904 (2011).
[12]I. I. Naumov and H. Fu, Phys. Rev. Lett. **95**, 247602 (2005).
[13]A. Schilling, R. M. Bowman, J. M. Gregg, G. Catalan, and J. F. Scott, Appl. Phys. Lett. **89**, 212902 (2006).
[14]J. F. Scott, Science **315**, 954 (2007).
[15]N. Setter, D. Damjanovic, L. Eng, G. Fox, S. Gevorgian, S. Hong, A. Kingon, H. Kohlstedt, N. Y. Park, G. B. Stephenson, I. Stolitchnov, A. K. Taganstev, D. V. Taylor, T. Yamada, and S. Streiffer, J. Appl. Phys. **100**, 051606 (2006).
[16]D. Sichuga and L. Bellaiche, Phys. Rev. B **85**, 214111 (2012).
[17]I. Naumov and A. M. Bratkovsky, Phys. Rev. Lett. **101**, 107601 (2008).
[18]W. J. Chen, Y. Zheng, and B. Wang, Appl. Phys. Lett. **100**, 062901 (2012).
[19]D. C. Ma, Y. Zheng, and C. H. Woo, Appl. Phys. Lett. **95**, 262901 (2009).
[20]G. Geneste, E. Bousquet, J. Junquera, and P. Ghosez, Appl. Phys. Lett. **88**, 112906 (2006).
[21]S. Tinte and M. G. Stachiotti, Phys. Rev. B **64**, 235403 (2001).
[22]J. Slutsker, A. Artemev, and A. Roytburd, Phys. Rev. Lett. **100**, 087602 (2008).
[23]I. Ponomareva, I. I. Naumov, and L. Bellaiche, Phys. Rev. B **72**, 214118 (2005).
[24]A. Schilling, D. Byrne, G. Catalan, K. G. Webber, Y. A. Genenko, G. S. Wu, J. F. Scott, and J. M. Gregg, Nano Lett. **9**, 3359 (2009).
[25]B. J. Rodriguez, X. S. Gao, L. F. Liu, W. Lee, I. I. Naumov, A. M. Bratkovsky, D. Hesse, and M. Alexe, Nano Lett. **9**, 1127 (2009).
[26]H. Fu and L. Bellaiche, Phys. Rev. Lett. **91**, 257601 (2003).
[27]S. Prosandeev and L. Bellaiche, Phys. Rev. B **75**, 094102 (2007).
[28]A. Schilling, S. Prosandeev, R. G. P. McQuaid, L. Bellaiche, J. F. Scott, and J. M. Gregg, Phys. Rev. B **84**, 064110 (2011).
[29]Y. Su and J. N. Du, Appl. Phys. Lett. **95**, 012903 (2009).
[30]I. Münch and J. E. Huber, Appl. Phys. Lett. **95**, 022913 (2009).
[31]L. Hong, A. K. Soh, S. Y. Liu, and L. Lu, J. Phys. D: Appl. Phys. **42**, 122005 (2009).
[32]G. Catalan, J. Seidel, R. Ramesh, and J. F. Scott, Rev. Mod. Phys. **84**, 119 (2012).
[33]A. Schilling, R. M. Bowman, G. Catalan, J. F. Scott, and J. M. Gregg, Nano Lett. **7**, 3787 (2007)
[34]S. M. Yang, Y. J. Shin, Y. Ehara, H. Funakubo, J. G. Yoon, J. F. Scott, and T. W. Noh, private communication (2012).
[35]Y. L. Li, S. Y. Hu, Z. K. Liu, and L. Q. Chen, Appl. Phys. Lett. **81**, 427 (2002).
[36]M. G. Stachiotti and M. Sepliarsky, Phys. Rev. Lett. **106**, 137601 (2011).
[37]S. Prosandeev, I. Ponomareva, I. Kornev, I. Naumov, and L. Bellaiche, Phys. Rev. Lett. **96**, 237601 (2006).
[38]Y. Zheng and C. H. Woo, Appl. Phys. A **97**, 617 (2009).
[39]C. H. Woo and Y. Zheng, Appl. Phys. A **91**, 59 (2008).
[40]A. K. Tagantsev, Ferroelectrics **375**, 19 (2008).
[41]M. J. Haun, E. Furman, S. J. Jang, H. A. McKinstry, and L. E. Cross, J. Appl. Phys. **62**, 3331 (1987).
[42]Y. L. Li, L. E. Cross, and L. Q. Chen, J. Appl. Phys. **98**, 064101 (2005).
[43]Y. L. Wang, A. K. Tagantsev, D. Damjanovic, N. Setter, V. K. Yarmarkin, and A. I. Sokolov, Phys. Rev. B **73**, 132103 (2006).

[44]L. D. Landau, E. M. Lifshitz, and L. P. Pitaevskii, *Electrodynamics of Continuous Media* (Oxford University Press, Oxford, 1984).
[45]G. B. Stephenson and M. J. Highland, Phys. Rev. B **84**, 064107 (2011).
[46]D. C. Ma, Y. Zheng, B. Wang, and C. H. Woo, Appl. Phys. Lett. **99**, 142908 (2011).
[47]A. M. Bratkovsky and A. P. Levanyuk, J. Comput. Theor. Nanosci. **6**, 465 (2009).
[48]R. Kretschmer and K. Binder, Phys. Rev. B **20**, 1065 (1979).
[49]T. Sluka, A. K. Tagantsev, D. Damjanovic, M. Gureev, and N. Setter, Nat. Commun. **3**, 748 (2012).
[50]J. Hlinka and P. Márton, Phys. Rev. B **74**, 104104 (2006).
[51]W. L. Zhong, Y. G. Wang, P. L. Zhang, and B. D. Qu, Phys. Rev. B **50**, 698 (1994).
[52]$\alpha_1 = 4.124(T - 388) \times 10^5$, $\alpha_{11} = -2.097 \times 10^8$, $\alpha_{12} = 7.974 \times 10^8$, $\alpha_{111} = 1.294 \times 10^9$, $\alpha_{112} = -1.950 \times 10^9$, $\alpha_{123} = -2.500 \times 10^9$, $\alpha_{1111} = 3.863 \times 10^{10}$, $\alpha_{1112} = 2.529 \times 10^{10}$, $\alpha_{1122} = 1.637 \times 10^{10}$, $\alpha_{1123} = 1.367 \times 10^{10}$, $Q_{11} = 0.1104$, $Q_{12} = -0.0452$, $Q_{44} = 0.0289$, $s_{11} = 7.47 \times 10^{-12}$, $s_{12} = -2.95 \times 10^{-12}$, $s_{44} = 18.42 \times 10^{-12}$, $G_{11} = 51 \times 10^{-11}$, $G_{12} = 0$, $G_{44} = G'_{44} = 1 \times 10^{-11}$, $\delta_i = 43 \times 10^{-9}$ and $\varepsilon_b \approx 4.425 \times 10^{-10}$ (SI units and T in K).
[53]S. Prosandeev, I. Ponomareva, I. Naumov, I. Kornev, and L. Bellaiche, J. Phys.: Condens. Matter **20**, 193201 (2008).